Supporting Information

Title Magnetothermal Multiplexing for Selective Remote Control of Cell Signaling

*Junsang Moon[†, ‡, §], Michael G. Christiansen[//], Siyuan Rao[‡, §], Colin Marcus[†, ¶], David C Bono[†], Dekel Rosenfeld[‡, §], Danijela Gregurec[‡, §], Georgios Varnavides[†, ‡, §], Po-Han Chiang[‡, §, #], Seongjun Park[‡, §, ††, ‡‡] and Polina Anikeeva[†, ‡, §, §§]***

† Department of Materials Science and Engineering, Massachusetts Institute of Technology, Cambridge, MA, USA
‡ Research Laboratory of Electronics, Massachusetts Institute of Technology, Cambridge, MA, USA
§ McGovern Institute for Brain Research, Massachusetts Institute of Technology, Cambridge, MA, USA
// Department of Health Sciences and Technology, Swiss Federal Institute of Technology, 8093 Zürich, Switzerland
¶ Computer Science and Artificial Intelligence Lab, Massachusetts Institute of Technology, Cambridge, MA, USA
# Institute of Biomedical Engineering, National Chiao Tung University, 1001 University Road, Hsinchu, Taiwan 30010
†† Department of Electrical Engineering and Computer Science, Massachusetts Institute of Technology, Cambridge, MA, USA
‡‡ Department of Bio and Brain Engineering, Korea Advanced Institute of Science and Technology, Daejeon 34141, Republic of Korea
§§ Department of Brain and Cognitive Sciences, Massachusetts Institute of Technology, Cambridge, MA, USA

Supplementary Video S1 | Thermographic imaging of selective magnetothermal control of two ferrofluid droplet described in **Figure 4**. Heat insulated two different ferrofluid droplet (10ul) was placed in the gap of toroidal electromagnet. (Scale bar = 1 cm). Video play speed was adjusted to 8.28X times.

Supplementary Video S2 | Finite element analysis of the expected temperature distribution around 1 μL droplets of ferrofluids of MNP_1 and MNP_2 in a model of a mouse brain exposed to the paired AMF_1 and AMF_2 conditions. Distance between droplets was varied from 0 mm to 4 mm. The threshold of TRPV1 activation (41.5 ºC) was marked as a plane.

Supplementary Videos S3-6 | Inverted microscope imaging of multiplexed cellular signaling control processed in **Figure 5.** (Scale bars = 40 μm)

Supplementary Videos S3 and S4 – Fe_3O_4 16.3nm exposed to 10kA/m 522kHz AMF_1 and 70kA/m 50kHz AMF_2, respectively.

Supplementary Videos S5 and S6 – $Co_{0.24}Fe_{2.76}O_4$ 18.6nm exposed to 10kA/m 522kHz AMF_1 and 70kA/m 50kHz AMF_2, respectively.

Dynamic hysteresis model

To investigate the dynamic magnetization response and hysteresis of single domain magnetic nanoparticles exposed to alternating magnetic fields, we conducted numerical calculations based on a dynamic hysteresis model implemented in Mathematica.[1,2] Dynamic hysteresis models are most appropriate at frequencies well below the period of precession of magnetic moments described by the Landau Lifshitz Gilbert (LLG) equation. Rather than describing this precession, they instead treat coherent reversal of single domain MNPs (SDMNP) moments as a thermally activated kinetic process. A function describing the energy of possible orientations of individual particle moments accounts for two main contributions: the anisotropy of a SDMNP and its Zeeman energy in the external field. The resulting energy landscape has local minima that can be envisioned to each entrap a subpopulation of the moments in an ensemble, with some escaping to the other minimum at a rate determined by the energy barrier separating the minima. The net magnetization of this ensemble is thus determined by the fraction of moments residing in each energy minimum, typically neglecting the effect of local Boltzmann distributions within the minima. Since Zeeman energy depends on the external field, which varies in time, the energy landscape is also time-variant. Consequently, the switching rate from one energy minimum to another varies periodically with the applied field. To simplify the model, magnetic anisotropy was approximated with an easy-aligned, effective uniaxial anisotropy. The anisotropy of a SDMNP and its Zeeman energy can be expressed in a form normalized to ambient thermal energy by defining the quantities σ and ξ as follows.

$$\sigma = \frac{KV}{k_B T}, \xi = \frac{M_s V B}{k_B T}$$

(K - magnetic anisotropy, V – magnetic nanoparticle volume, k_B – Boltzmann constant, T – 298 K room temperature, M_S – saturation magnetization, B – applied field)

For cobalt doped ferrite ($Co_xFe_{3-x}O_4$) nanoparticles, magnetic anisotropy does not vary linearly depending on Co^{2+} concentration.[3] In our dynamic hysteresis calculations, values of K of cobalt doped ferrite MNPs were estimated from literature.[3,4]

Our dynamic hysteresis model followed previous work with some variations, and more detailed descriptions of this dynamic hysteresis model can be found there.[1,2] Unlike the previous work,[1,2] here the pre-exponential factor of relaxation time, τ_0, was not fixed to 10^{-9} s in order to reflect the fact that the pre-exponential factor is expected to vary with the anisotropy of SDMNP and the external field.[5,6] From the LLG equation, neglecting stochastic thermal effects, characteristic relaxation time (τ_c) is shorter for higher applied field ($\tau_c \propto \xi^{-1}$).[6] By considering this correlation[6] and the dependency of pre-exponential factor of Néel relaxation

on anisotropy of the SDMNP in the Fokker-Planck equation,[5] the pre-exponential factor τ_0 was made proportional to $\sigma^{-\frac{3}{2}}\xi^{-1}$. According to Leliaert at al., τ_0 is varies between 10^{-8} to 10^{-12} s for Fe_3O_4.[7] Consistent with this work, our τ_0 was multiplied by a suitable constant to place it within the same range:

$$\tau_0 = (2.045982 \times 10^{-7}\text{s}) \cdot \sigma^{-\frac{3}{2}}\xi^{-1}$$

Moreover, to account for the actual particle size distribution, each MNP ensemble's mean diameter and standard deviation were used to generate 100 random particles with a Gaussian distribution. The σ and ξ values corresponding to this statistical sample of particles were entered into our numerical model and the resulting magnetization responses were averaged to generate a population-averaged dynamic hysteresis loop.

Calculation of magnetic diameter

Magnetic particles are freely suspended in water, enabling continuous alignment of their moments with the applied field via physical rotation. This allows the magnetic diameter of a reasonably monodisperse particle ensemble to be determined under the assumption that the ensemble exhibits ideal superparamagnetic behavior in the limit of low applied fields. (The fitting technique employed here in the limit of low fields works equally well for fixed particles exhibiting anisotropy, provided they are randomly oriented. [2])

$$M_{experiment}(\xi) = M_{s-experiment} \times L(\xi),$$

Where $L(\xi)$ is the Langevin function, and $\xi \equiv \frac{\mu_m B}{k_B T}$,

$$(\mu_m = M_{s-theoretical} \times V_m, V_m \text{ is the magnetic volume})$$

For a magnetic field approaching $B \sim 0$ mT ($\xi \sim 0$), the Langevin function is approximately linear

$$M_{experiment}(\xi) \approx M_{s-experiment} \times \frac{\mu_m B}{3k_B T}$$

Therefore,

$$\frac{M_{experiment}(\xi)}{M_{s-experiment}} = \frac{V_m M_{s-theoretical}}{3k_B T} B$$

$$\frac{d\left(\frac{M_{experiment}(\xi)}{M_{s-experiment}}\right)}{dB} = \frac{V_m M_{s-theoretical}}{3k_B T} = slope$$

The magnetic diameter d_m can then be determined from the magnetic volume:

$$V_m = \frac{4}{3}\pi\left(\frac{d}{2}\right)^3$$

$$d_m = \sqrt[3]{\frac{18k_B T \times slope}{\pi M_{s-theoretical}}}$$

To maintain $\xi \sim 0$ condition, which is required for an accurate linear Taylor approximation of $L(\xi)$, the cutoff for the fitted region of magnetic field strength should be varied depending on the particle size since the magnetic moment μ_m changes dramatically depending on the particle size. Therefore, the slope of M/M_s vs. B was fitted within different magnetic field strength

ranges (Fe_3O_4, 16.3 nm: –2~2 mT, 20.5 nm: –1~1 mT, 25.2 nm: –0.5~0.5 mT and 31.2 nm: –0.4~0.4 mT).

For cobalt doped ferrite ($Co_xFe_{3-x}O_4$) nanoparticles, M_S was determined from the Vegard's Law, which follows a linear regression line between $M_S^{Fe_3O_4}$ and $M_S^{CoFe_2O_4}$.[3] ($Co_xFe_{3-x}O_4$, x=0.01: -0.5~0.5mT, x=0.03: -0.4~0.4mT, x=0.12: -1.1mT~1.1mT, x=0.24: -2~2mT).

Multiplexing factor (MF) for selecting AMF conditions

We analyzed AC magnetometry data to identify the AMF conditions most suitable for magnetothermal multiplexing with the selected MNP ensembles. Multiplexing requires not only that each ferrofluid should heat up effectively in one AMF condition, but also that it dissipates minimal heat in the other AMF condition. To quantitatively evaluate selectivity, we defined the ratio of specific loss powers of a particular MNP ensemble at different AMF conditions as *Selectivity (S)*. If MNP_1 is the low-K_{eff} MNP (less coercive), intended to dissipate more heat in AMF_1 with low amplitude (H_1) and high frequency (f_1) than in AMF_2 with high amplitude (H_2) and low frequency (f_2), while high-K_{eff} MNP_2 (more coercive) will generate more heat when exposed to AMF_2, then *S* can be formulated as:

$$S_{MNP_1}(H_1, f_1, H_2, f_2) = \begin{cases} \dfrac{\mathrm{SLP}_{MNP_1}(H_1, f_1)}{\mathrm{SLP}_{MNP_1}(H_2, f_2)} & \text{for } H_2 > H_1 \text{ and } f_2 < f_1 \\ 0 & Otherwise \end{cases}$$

$$S_{MNP_2}(H_1, f_1, H_2, f_2) = \begin{cases} \dfrac{\mathrm{SLP}_{MNP_2}(H_2, f_2)}{\mathrm{SLP}_{MNP_2}(H_1, f_1)} & \text{for } H_2 > H_1 \text{ and } f_2 < f_1 \\ 0 & Otherwise \end{cases}$$

S is set to 0 for AMF pairs for which both amplitude and frequency of one condition exceed the other, because MNPs in the dominant AMF will always dissipate more heat than the other AMF, which runs contrary to the purpose of magnetothermal multiplexing.

S of the ferrofluid of MNP_1 can be maximized under conditions in which low-amplitude, high-frequency AMF_1 allows access to the major hysteresis loops of the material and cycles rapidly enough to produce substantial heat dissipation. Conversely, the high-amplitude, low-frequency AMF_2, while also sufficient in magnitude to drive major hysteresis loops for MNP1, cycles through these loops at a significantly lower rate and hence results in lower heat dissipation. In contrast, the ferrofluid of MNP_2, with its higher coercivity dissipates negligible heat in low-amplitude, high-frequency AMF_1, which is insufficient to access its major hysteresis loops, but exhibits large hysteresis loop area at high-amplitude, low-frequency AMF_2.

Simply multiplying S_{MNP_1} and S_{MNP_2} may seem to be an expedient approach to define the overall multiplexing selectivity for this materials pair. However, this can misleadingly identify AMF_1 and AMF_2 conditions in which particularly high selectivity for one MNP ensemble veils the far less selective operation of the other MNP ensemble. To avoid such scenarios, we introduce $Equity$ (E), defined as a ratio of the geometric and arithmetic means:

$$E = \frac{\sqrt{S_{MNP_1} \cdot S_{MNP_2}}}{\frac{S_{MNP_1} + S_{MNP_2}}{2}}$$

This quantity ranges between 0 and 1 and approaches 1 as S_{MNP1} and S_{MNP2} values approach each other, producing the exclusion of AMF conditions (H_1, f_1, H_2, f_2) that yield imbalanced S_{MNP1} and S_{MNP2}. An overall *Multiplexing Factor (MF)* is then defined as:

$$MF(H_1, f_1, H_2, f_2) = S_{MNP_1} \cdot S_{MNP_2} \cdot E = 2\frac{\left(S_{MNP_1} \cdot S_{MNP_2}\right)^{3/2}}{S_{MNP_1} + S_{MNP_2}}$$

Finding paired AMF conditions

Since differing coercivity is the basis for multiplexing in this material system, we began by selecting the two batches of magnetic nanoparticles that showed the largest difference in coercivity. To find optimized multiplexed condition, we introduced a *multiplexing factor (**MF**)*, which depends on four parameters (H_1,f_1, H_2, f_2, where H_x and f_x are amplitude and frequency of AMF_x, respectively).

$$MF(H_1, f_1, H_2, f_2)\ H_x - \text{Field amplitude of AMF}_x, f_x - \text{ frequency of AMF}_x$$

Since these four parameters can vary independently, in the most general case they define a four-dimensional parameter space over which $\boldsymbol{MF}$ varies. To find optimally paired AMF conditions, parameters that maximize $\boldsymbol{MF}$ should be identified. Hysteresis loops do not vary markedly with frequency for MNPs driven by AMFs in the frequency range of interest. [8–11] This has two notable consequences: 1) A reduced three dimensional parameter space is possible in terms of H_1 , H_2 , and the ratio f_1/f_2. 2) It is feasible to determine SLP versus amplitude curves for MNP_1 and MNP_2 throughout this space based on characterization at one frequency. We took the further step of fitting these curves with analytical functions using a non-linear least square fit. (The logistic functions assumed for this fit do not have any physical meaning but converged well to the data and offered simple analytic expressions for scanning over parameters.) (**Supplementary Figure 3 and Supplementary Table 1**)

$$SLP(H) = a \cdot \frac{1}{1 + e^{-b \cdot (H-c)}} \quad (a, b \text{ and } c \text{ are constants})$$

A global maximum for preliminary *MF* subject to these constraints was determined for H_1 = 11.1 kA/m, H_2 = 70 kA/m, and f_1/f_2 = 10.72. From this result, AMF generator was built to have

frequency pairs, 522 kHz and 50 kHz (f_1/f_2 = 10.44), where all chosen AMF conditions exhibit amplitude-frequency products near or below AMF safety limit. ($H \cdot f < 5\times10^9$ $Am^{-1}\cdot s^{-1}$)[12]

To determine final AMF conditions for multiplexing, $MF(H_1, 522\ kHz, H_2, 50\ kHz)$ constructed out of SLP profile from AC magnetometer was scanned over AMF amplitudes space. (H_1 and H_2) (**Figure 4** and **Supplementary Figure 4**) From this scanning, final AMF conditions were set to H_1 =10 kA/m, f_1 =522 kHz and H_2 =70 kA/m, f_2 =50 kHz.

Multiplexing performance of the selected MNPs at the selected AMF conditions

In AMF_1 (H_1 =10 kA/m and f_1 =522 kHz), MNP_1 (16.3 nm Fe_3O_4) and MNP_2 (18.6 nm $Co_{0.24}Fe_{2.76}O_4$) exhibited $SLP_{MNP_1}(AMF_1)$ = 203 W/g and $SLP_{MNP_2}(AMF_1)$ = 50 W/g, respectively. In contrast, in AMF_2 (H_2 =70 kA/m and f_2 =50 kHz), higher coercivity particles produced significantly more heat with the corresponding values of $SLP_{MNP_1}(AMF_2)$ = 53 W/g and $SLP_{MNP_2}(AMF_2)$ = 369 W/g. Together these values returned a multiplexing factor MF = 26.81.

Finite element analysis of the heat dissipation from the adjacent ferrofluid droplets

To determine the minimal distance that prevents crosstalk between two adjacent ferrofluid droplets acting as heat sources inside a model system of a mouse brain, we applied a finite element model of heat transport.

Pennes' bio-heat equation was used to account for the influence of blood perfusion within the brain tissue:

$$\rho_B C_B \frac{\partial T}{\partial t} = K_B \nabla^2 T + \rho_b C_b w_b (T - T_b) + Q$$

Where ρ_B, ρ_b and C_B, C_b are densities and heat capacities of the brain and blood, respectively; K_B is the thermal conductivity of the brain; T_b is blood temperature; and w_b is the cerebral blood flow. Q is the power density of the heat source, and T – temperature.

Two distinct ferrofluid injections (MNP_1 and MNP_2) inside the brain tissue were approximated as spheres acting as sources of constant power density Q due to the AMF. We calculated the temperature profile of the tissue as a function of time. The physical parameters used in our model are summarized in the **Supplementary Table S2**. Q was calculated as:

$$Q = V_{MNP} * SLP_{MNP} * \rho_{MNP}$$

where V_{MNP} is the total volume of MNPs in the droplet, ρ_{MNP} is the concentration of MNPs and SLP_{MNP} is the specific loss power for the MNPs in the examined AMF conditions of f_1 = 522 kHz, H_1 = 10 kA/m and f_2 = 50 kHz or H_2 = 70 kA/m. SLPs for MNP_1 and MNP_2 from the thermographic recording (Figure 4) were used in this model (**Supplementary Table S3**).

Prior research indicates that injected MNPs coated with mPEG-PMAO polymer stay mainly within injected area, even after a month. [13] Therefore, in our model, we also assumed that injected ferrofluids will maintain their shapes.

To assess the minimal distance required for selective heat control, we ran multiple simulations at varying distances between ferrofluid droplets (d = 0, 1, 2, 3, 4 mm) (**Supplementary Video S2** and **Supplementary Figure S7**). In our model, an AMF with f_1 = 522 kHz, H_1 = 10 kA/m was applied for the first 20s, followed by a 60s rest epoch, then another AMF with f_2 = 50 kHz, H_2 = 70 kA/m was applied for 20s, followed by another 60s rest (**Supplementary Figure S7a**).

As the distance between the droplets exceeds 2 mm, the regions of elevated temperature

generated by two ferrofluid droplets are clearly separated (**Supplementary Video S2** and **Supplementary Figure S7a,b**). This suggests that the multiplexed magnetothermal system can target nearby organ regions such as distinct areas of the brain even in small rodents (**Supplementary Figure S7c,d**).

Supplementary Table S1 | Curve fitting results for SLP data of MNP_1 and MNP_2 collected using the AC magnetometer.

	a	b	c	R-square	RMSE
MNP_1	1180	-0.08	62.19	0.9671	7.5426
MNP_2	112.4	-0.12	16.42	0.9980	16.8423

Supplementary Table S2 | Physical parameters used in the FEM modeling.

Parameter	**Value**
Blood density, ρ_b	1050 kg/m^3 [13]
Blood specific heat capacity, $C_{p,b}$	3617 J/(kg·K) [13]
Cerebral blood flow, ω_b	1.07ml/g/min [14]
Arterial blood temperature, T_b	37 °C [13]
Initial and boundary temperature, T_0	37 °C [13]
Brain specific heat capacity, $C_{p,B}$	3630 J/(kg·K) [13]
Brain density, ρ_B	1065 kg/m^3 [13]
Brain thermal conductivity, K_B	0.51 W/(m·K) [13]
Fe_3O_4 ferrofluid concentration	115.534 mg_{Metal}/ml
$Co_{0.24}Fe_{2.76}O_4$ ferrofluid concentration	64.674 mg_{Metal}/ml

Supplementary Table S3 | The summary table of SLP measurements for multiplexed magnetothermal experiments.

Field condition	**AMF_1 (522 kHz, 10 kA/m)**		**AMF_2 (50 kHz, 70 kA/m)**	
Particle	**MNP_1**	**MNP_2**	**MNP_1**	**MNP_2**
AC magnetometer	203 W/g_{Metal}	50 W/g_{Metal}	53 W/g_{Metal}	369 W/g_{Metal}
Thermographic recording	206 W/g_{Metal}	59 W/g_{Metal}	43 W/g_{Metal}	368 W/g_{Metal}
In vitro	202 W/g_{Metal}	65 W/g_{Metal}	47 W/g_{Metal}	369 W/g_{Metal}

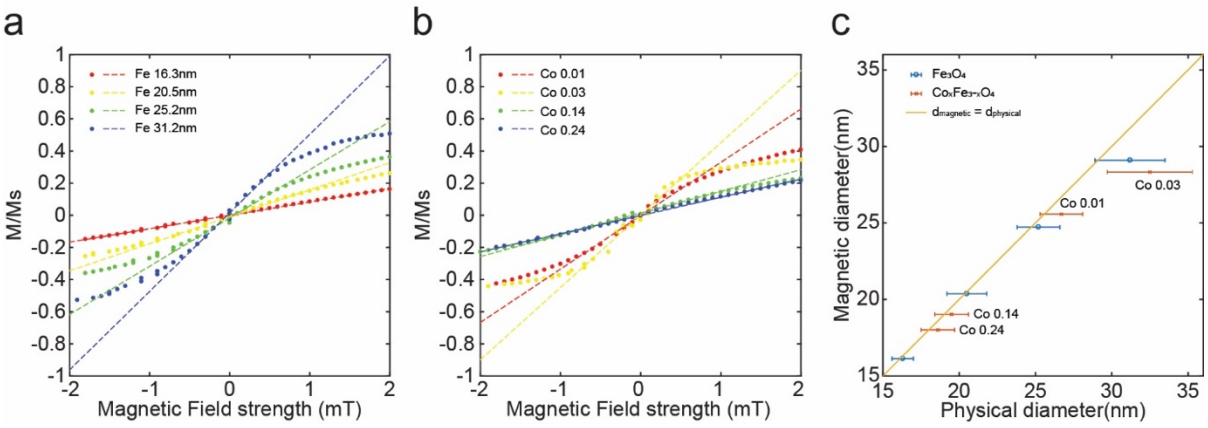

Supplementary Figure S1 | Magnetic and physical diameter of MNP ensembles. Normalized magnetization curves collected via vibrating sample magnetometry (VSM) vs. applied magnetic field for Fe_3O_4 (**a**) and $Co_xFe_{3-x}O_4$. (**b**). **c**, Summary of MNP physical diameters obtained from TEM images vs. magnetic diameters calculated from the VSM curves. Quantitative agreement between physical and magnetic diameters suggests that MNPs exhibit saturation magnetization values approaching those of bulk materials and therefore possess monocrystalline inverted spinel structure.

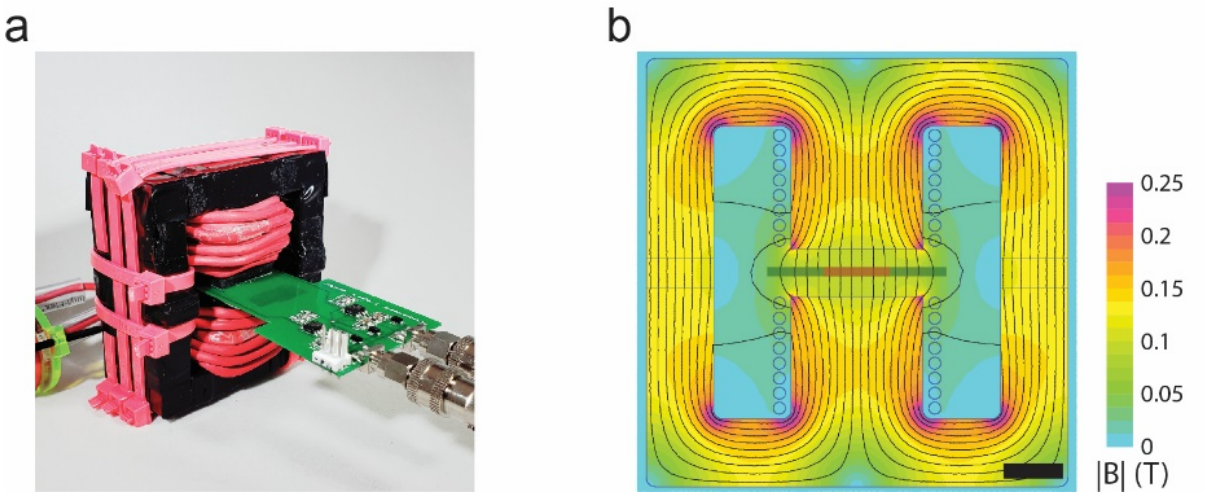

Supplementary Figure S2 | AC magnetometer assembly and magnetic flux density plot. a, AC magnetometer assembly composed of AC magnetometer board and AMF generator. **b**, Simulated magnetostatic flux density plot calculated via Finite Element Method for Magnetics (FEMM). Our two-dimensional (2D) AC magnetometer is placed in the center of the magnetic core gap with 5 mm margin to every edge to ensure field uniformity. (Black line – scale bar = 1 cm, green line – PCB plate, red line – spiral coil sensor).

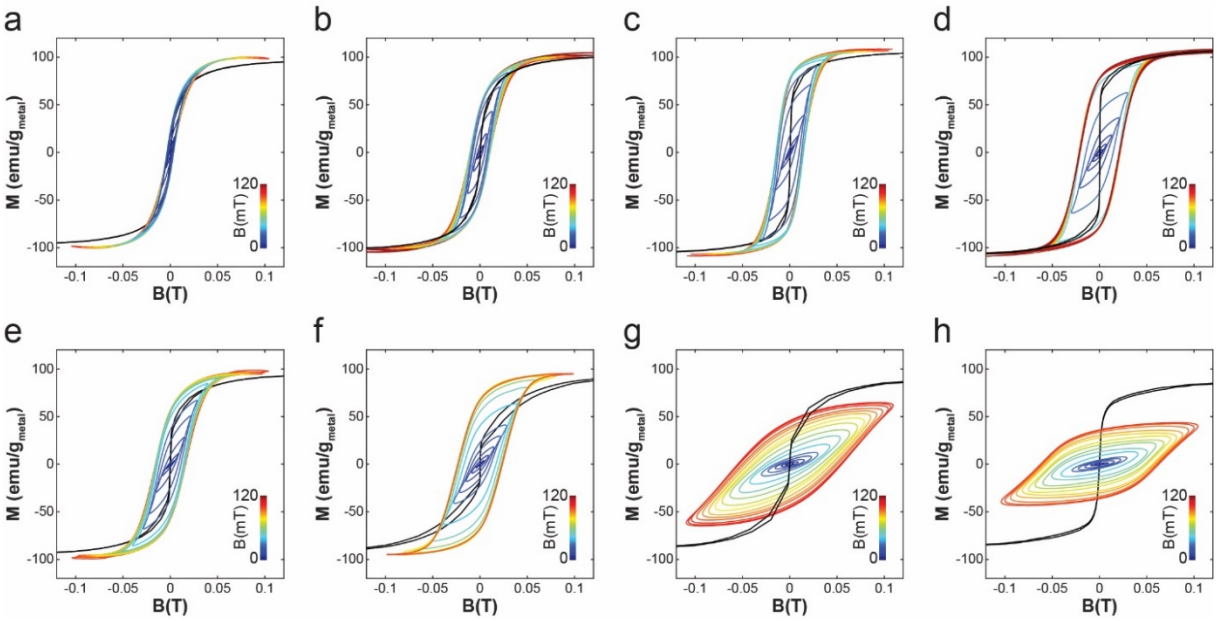

Supplementary Figure S3 | Dynamic magnetization measurements for 8 ferrofluids. a-d, Fe_3O_4 (**a,** 16.3nm; **b,** 20.5nm; **c,** 25.2nm; **d,** 31.2nm). **e-h,** $Co_xFe_{3-x}O_4$ (**e,** x=0.01, 26.7nm; **f,** x=0.03 32.5nm; **g,** x=0.14 19.5nm; **h,** x=0.24 18.6nm). Black lines correspond to VSM data, rainbow colored loops correspond to custom-built AC magnetometer data. All data were collected at a frequency f = 75 kHz.

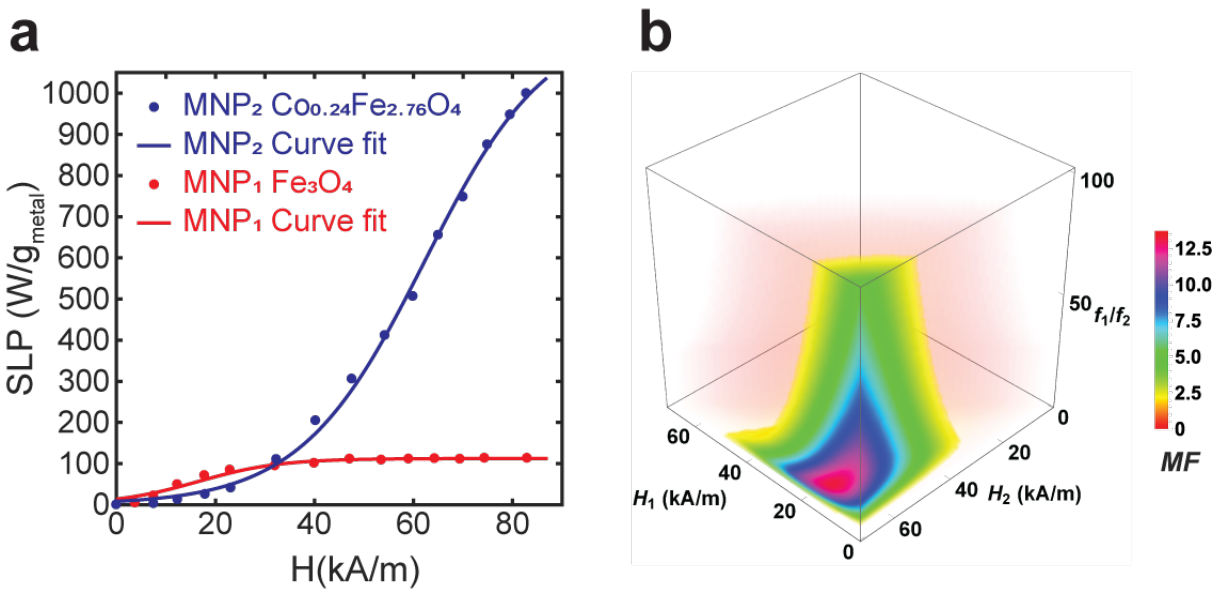

Supplementary Figure S4 | Initial selection of AMF conditions for magnetothermal multiplexing using analytically defined Multiplexing Factor. a, Curve fitting of the SLP values recorded for Fe_3O_4 16.3nm and $Co_{0.24}Fe_{2.76}O_4$ 18.6 nm MNPs. **b,** Multiplexing Factor plotted as a function of AMF amplitudes (H_1 and H_2) and frequency ratio (f_1/f_2) to determine initial AMF conditions prior to further experimental refinement.

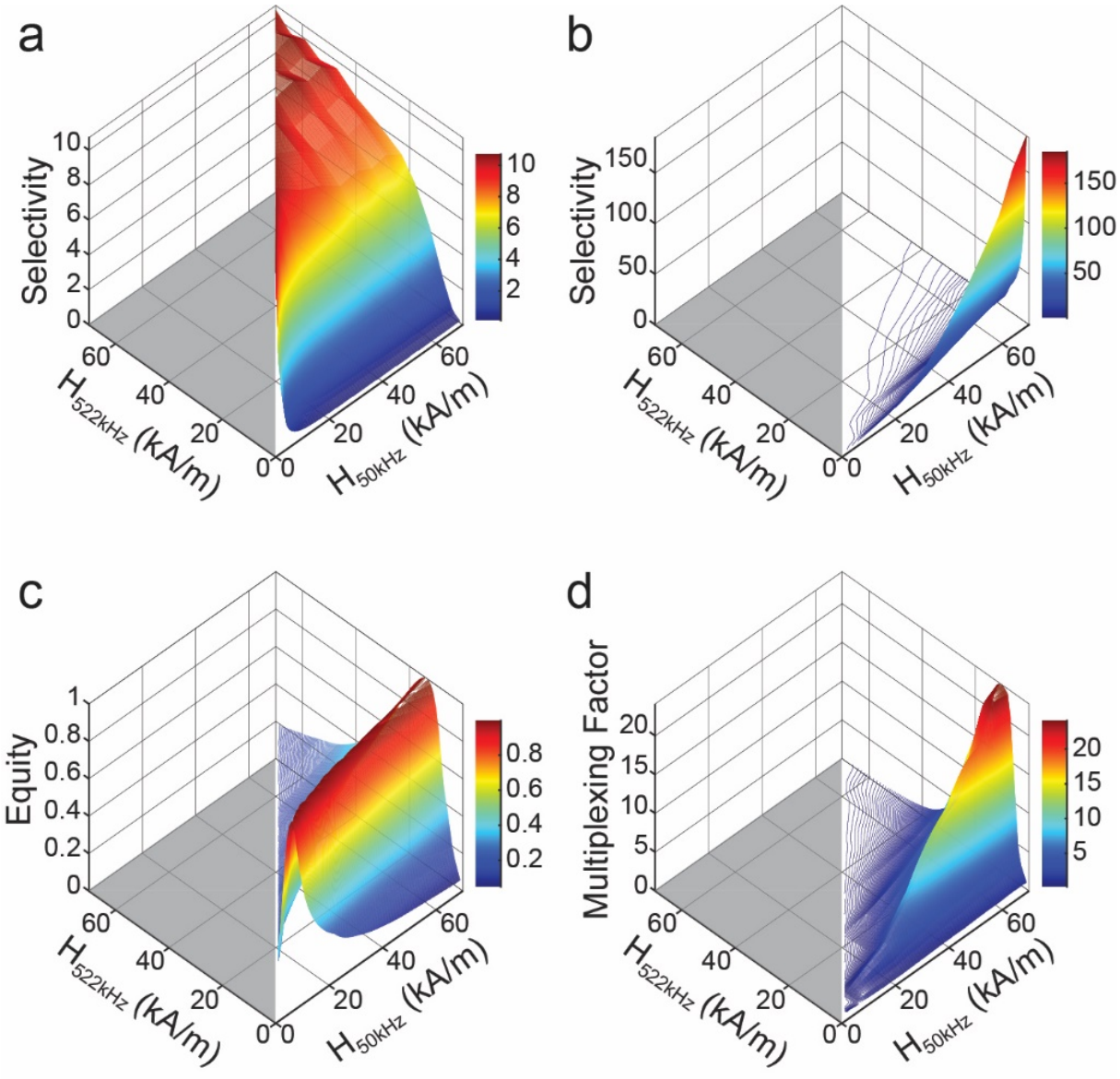

Supplementary Figure S5 | Optimization of AMF amplitudes for magnetothermal multiplexing. Grey areas correspond to unsuitable conditions (selectivity, $S = 0$). **a, b,** Selectivity of Fe_3O_4 16.3nm **(a)** and$Co_{0.24}Fe_{2.76}O_4$ 18.6 nm **(b)** MNPs as a function of AMF amplitudes between 0-70 kA/m (accessible in our apparatus) and frequencies of 522 kHz and 50 kHz. **c,** Equity between the two MNP ensembles as a function of AMF amplitudes between 0-70 kA/m (accessible in our apparatus) and frequencies of 522 kHz and 50 kHz. **d,** Multiplexing Factor as a function of AMF amplitudes between 0-70 kA/m (accessible in our apparatus) and frequencies of 522 kHz and 50 kHz.

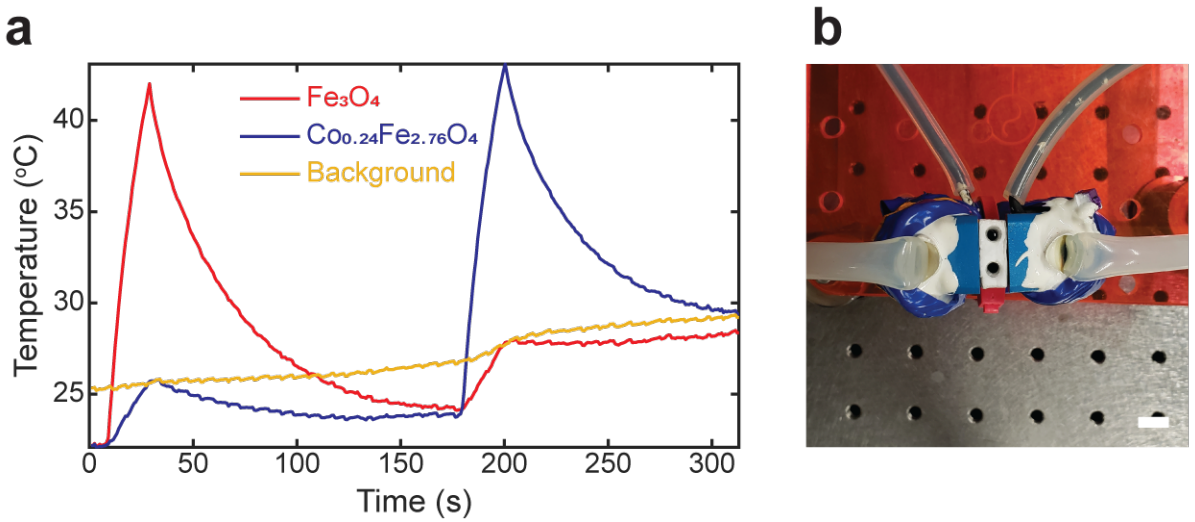

Supplementary Figure S6 | Experiment demonstrating the selective heating of two neighboring ferrofluid droplets. a, Temperature profiles for Fe_3O_4 16.3nm and $Co_{0.24}Fe_{2.76}O_4$ 18.6 nm ferrofluid droplets as well as the background (water). **b,** Top view of AMF generating gapped toroid electromagnet (scale bar = 1 cm).

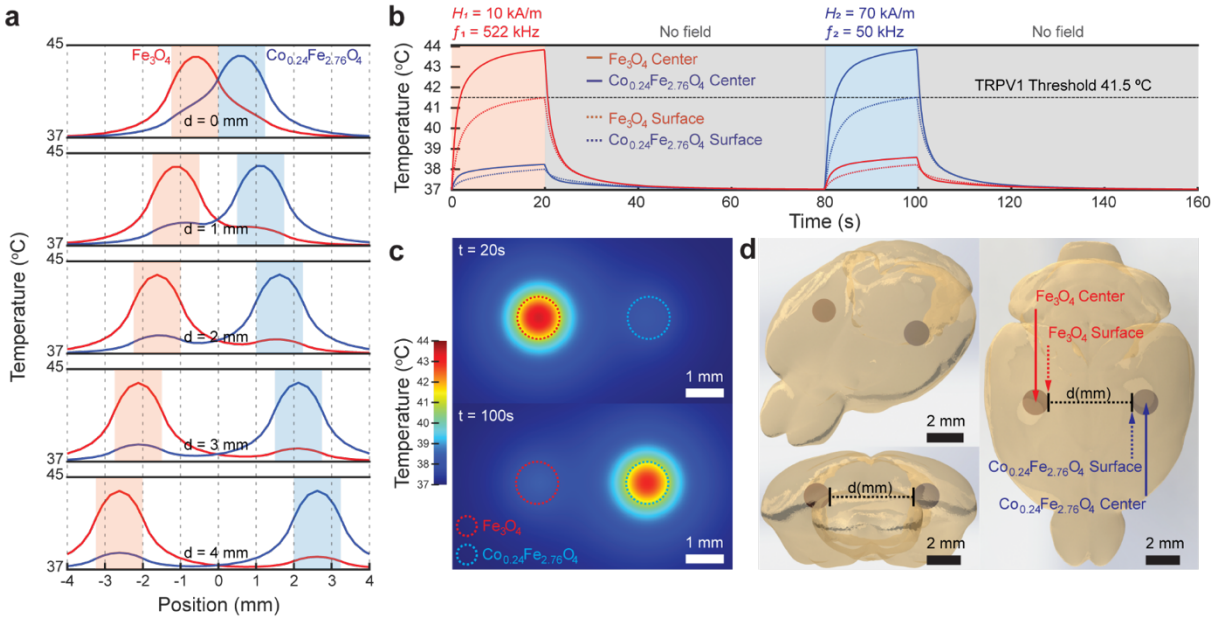

Supplementary Figure S7 | Temperature distribution for the two multiplexed ferrofluid droplets injected within the brain tissue and exposed to the tailored AMF conditions. a, Temperature profiles for MNP_1 (Fe_3O_4, red) and MNP2 ($Co_{0.24}Fe_{2.76}O_4$, blue) along centers of the ferrofluid droplets separated by distance d = 0, 1, 2, 3, 4 mm between their surfaces. Shaded areas mark the droplet positions (red - Fe_3O_4, blue – $Co_{0.24}Fe_{2.76}O_4$) **b**, Temperature profile of each droplet at the center and on the surface over time (d = 2 mm). **c**, Heat maps of the ferrofluid droplets within the brain tissue at t = 20 s and t = 100s (d = 2 mm). **d**, Three-dimensional view of the ferrofluid droplets injected in the different hemispheres of the mouse brain.

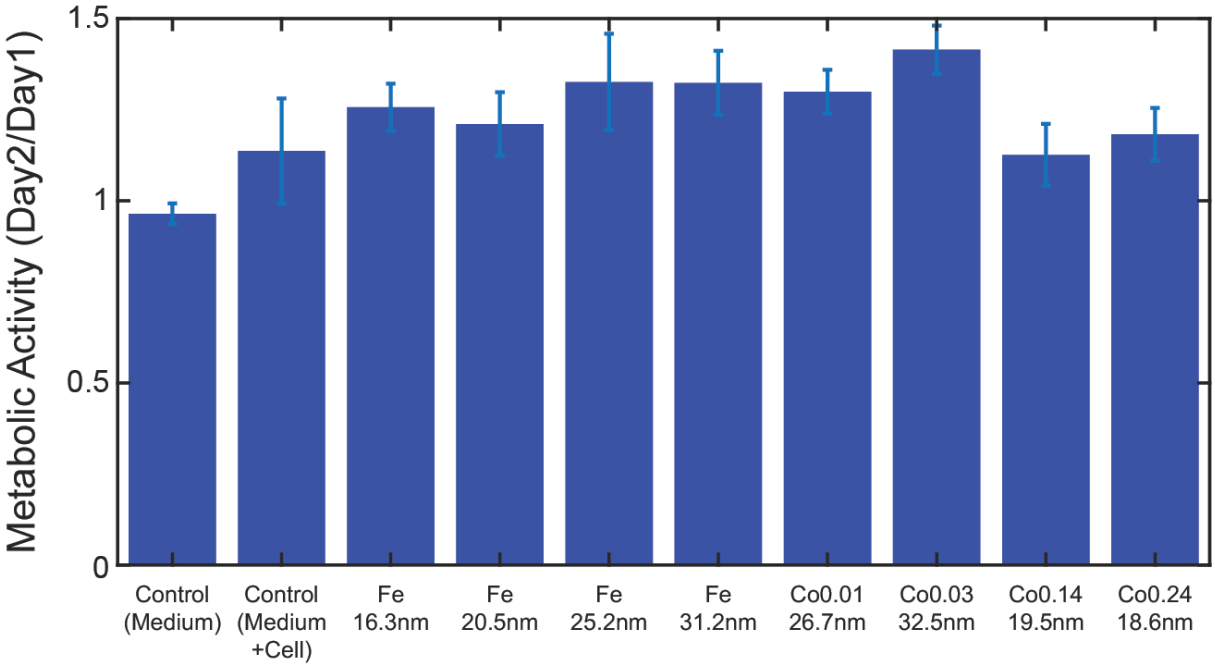

Supplementary Figure S8 | Biocompatibility of magnetic nanoparticles in HEK239T cell cultures. Proliferation of HEK293T in ferrofluid media was tested by Alamar Blue assay. Each well was tested without MNPs on day 1 and with MNPs on day 2. (Number of samples n=4, error bars represent standard deviation).

Supplementary references

[1] M. G. Christiansen, A. W. Senko, R. Chen, G. Romero, P. Anikeeva, *Appl. Phys. Lett.* **2014**, *104*, 213103.

[2] J. Carrey, B. Mehdaoui, M. Respaud, *J. Appl. Phys.* **2011**, *109*.

[3] M. Tachiki, *Prog. Theor. Phys.* **1960**, *23*, 1055.

[4] R. C. O'Handley, *Modern magnetic materials: principles and applications*; Wiley, 2000.

[5] R. J. Deissler, Y. Wu, M. A. Martens, *Med. Phys.* **2016**, *41*, 12301.

[6] D. B. Reeves, J. B. Weaver, *Appl. Phys. Lett.* **2014**, *104*, 102403.

[7] J. Leliaert, A. Coene, G. Crevecoeur, A. Vansteenkiste, D. Eberbeck, F. Wiekhorst, B. Van Waeyenberge, L. Dupré, *J. Appl. Phys.* **2014**, *116*, 163914.

[8] E. Garaio, J. M. Collantes, J. A. Garcia, F. Plazaola, S. Mornet, F. Couillaud, O. Sandre, *J. Magn. Magn. Mater.* **2014**, *368*, 432.

[9] E. Garaio, J. M. Collantes, F. Plazaola, J. A. Garcia, I. Castellanos-Rubio, *Meas. Sci. Technol.* **2014**, *25*.

[10] C. Guibert, J. Fresnais, V. Peyre, V. Dupuis, *J. Magn. Magn. Mater.* **2017**, *421*, 384.

[11] H. Kobayashi, K. Ueda, A. Tomitaka, T. Yamada, Y. Takemura, *IEEE Trans. Magn.* **2011**, *47*, 4151.

[12] R. Hergt, S. Dutz, *J. Magn. Magn. Mater.* **2007**, *311*, 187.

[13] R. Chen, G. Romero, M. G. Christiansen, A. Mohr, P. Anikeeva, *Science* **2015**, *347*, 1477.

[14] E. R. Muir, Q. Shen, T. Q. Duong, *Magn. Reson. Med.* **2008**, *60*, 744.